J Biol Inorg Chem (2008) 13:899–907
DOI 10.1007/s00775-008-0377-4

ORIGINAL PAPER

Electron paramagnetic resonance characterization of the copper-resistance protein PcoC from *Escherichia coli*

Simon C. Drew · Karrera Y. Djoko · Lianyi Zhang · Melissa Koay · John F. Boas · John R. Pilbrow · Zhiguang Xiao · Kevin J. Barnham · Anthony G. Wedd

Received: 31 December 2007 / Accepted: 5 April 2008 / Published online: 18 April 2008

Abstract Continuous-wave and pulsed electron paramagnetic resonance have been applied to the study of the Cu^{II} site of the copper-resistance protein PcoC from *Escherichia coli* and certain variant forms. Electron spin echo envelope modulation (ESEEM) experiments confirm the presence of two histidine ligands, His1 and His92, at the Cu^{II} site of wild-type PcoC, consistent with the available X-ray crystallographic data for the homolog CopC (67% sequence identity) from *Pseudomonas syringae* pv. *tomato*. The variants H1F and H92F each lack one of the histidine residues close to the Cu^{II} site. The ESEEM data suggest that the surviving histidine residue remains as a ligand. The nA variant features an extra alanine residue at the N terminus, which demotes the His1 ligand to position 2. At least one of the two histidine residues is bound at the Cu^{II} site in this form. Simulation of the ^{14}N superhyperfine structure in the continuous-wave spectra confirms the presence of at least three nitrogen-based ligands at the Cu^{II} sites of the wild-type, H92F and nA forms, while the H1F variant has two nitrogen ligands. The spectra of wild-type form can be fitted adequately with a 3N or a 4N model. The former is consistent with the crystal structure of the CopC homolog, where His1 acts as a bidentate ligand. The latter raises the possibility of an additional unidentified nitrogen ligand. The markedly different spectra of the H1F and nA forms compared with the wild-type and H92F proteins further highlight the integral role of the N-terminal histidine residue in the high-affinity Cu^{II} site of PcoC.

Keywords Copper transport · Copper proteins · Electron paramagnetic resonance · Electron spin echo envelope modulation · Hyperfine sublevel correlation experiment

Abbreviations

CW	Continuous wave
EPR	Electron paramagnetic resonance
ESEEM	Electron spin echo envelope modulation
HYSCORE	Hyperfine sublevel correlation experiment

Introduction

Some strains of *Escherichia coli* can survive in copper-rich environments that would normally overwhelm the chromosomal copper tolerance system [1]. Such strains possess additional plasmid-encoded genes that confer copper resistance. A well-documented example was found in the feces of copper-fed pigs and its resistance was attributed to a plasmid-borne *pco* operon comprising seven genes,

Electronic supplementary material The online version of this article (doi:10.1007/s00775-008-0377-4) contains supplementary material, which is available to authorized users.

S. C. Drew (✉) · K. J. Barnham
Department of Pathology,
Bio21 Molecular Science and Biotechnology Institute,
University of Melbourne,
Parkville, VIC 3010, Australia
e-mail: sdrew@unimelb.edu.au

K. Y. Djoko · L. Zhang · M. Koay · Z. Xiao · A. G. Wedd
School of Chemistry,
Bio21 Molecular Science and Biotechnology Institute,
University of Melbourne,
Parkville, VIC 3010, Australia

S. C. Drew · J. F. Boas · J. R. Pilbrow
School of Physics,
Monash University,
Clayton, VIC 3800, Australia

pcoABCDpcoRSpcoE [2–4]. Equivalent copper-resistance operons *copABCDcopRS* have been found in copper-resistant strains of *Pseudomonas syringae* pv. *tomato* isolated from plants exposed to high levels of copper compounds [5]. High copper levels induce expression of the proteins which operate in the periplasmic space to confer copper resistance [4–7].

CopC and PcoC are small soluble β-barrel proteins which are expressed from the abovementioned operons [5, 8]. They exhibit two separated binding sites which are specific for Cu^{I} and Cu^{II} [9–11]. In addition, X-ray crystallography supported the conclusion that the sites in CopC feature the following ligands: $[Cu^{I}(His)(Met)_{2,3}]$ and $[Cu^{II}(His)_2(N\text{-term})(OH_2)]$ (Fig. 1) [12]. The Cu^{II} site uses the amino terminus as a ligand, making His1 effectively a bidentate ligand [12], a situation observed previously only in simple Cu^{II}–peptide complexes [13–15].

Production of variant proteins demonstrated that the two copper binding sites are interdependent and that they can effect intermolecular transfer from either site with or without change of oxidation state [12]. Such transfers require the availability of a high-affinity binding site to receive the transported ion. Overall, the properties of CopC and PcoC are consistent with those expected of versatile copper carriers interacting directly with other members of their protein families to confer copper resistance. Indeed, Cu^{I} bound to PcoC is oxidized to less toxic Cu^{II} by the multi-copper oxidase PcoA, a likely biological partner [16].

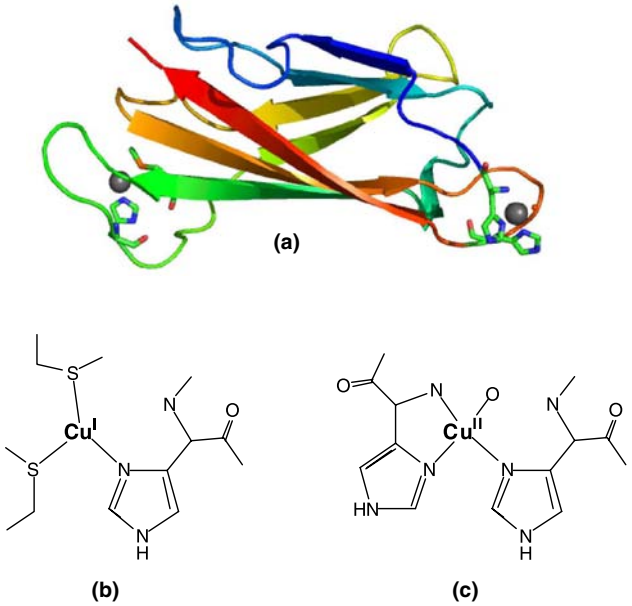

Fig. 1 **a** Ribbon representation of PcoC and CopC proteins determined from X-ray crystallography of the CopC homolog [12]. Two-dimensional representation of the **b** Cu^{I} and **c** Cu^{II} sites

Although CopC and PcoC share 67% sequence identity, significant differences in properties were reported initially [8, 9, 11, 12, 17, 18]. The differences were traced to the presence of an additional N-terminal alanine residue in the PcoC protein as expressed initially [19]. Consequently, His1 was demoted to position 2, a situation which altered the nature of the Cu^{II} binding site (Fig. 1c) dramatically in this form of the protein (designated nA-PcoC). Electron paramagnetic resonance (EPR) was among the range of techniques used initially to characterize the Cu^{II} (d^9) site in nA-PcoC [8]. The present paper reports a comparison of the EPR properties of the bona fide wild-type PcoC protein with those of the nA-PcoC protein, as well as the variant forms (H1F, H92F) in which these ligand side chains are replaced by nonligating benzyl side chains.

Materials and methods

Proteins and reagents

Native and variant PcoC proteins (apo, Cu^{II} and $Cu^{I}Cu^{II}$ forms) and nA-PcoC were isolated and handled as reported previously [12, 19] and prepared in 20 mM potassium phosphate, 100 mM NaCl, pH 7. Approximately 10% v/v glycerol was added as a cryoprotectant.

A $^{65}CuCl_2$ stock was generated by dissolving ^{65}CuO (99%+; Cambridge Isotopes) in concentrated HCl, stirring under heat for 8 h and diluting in distilled water to a final concentration of 30 mM. Protein samples enriched in ^{65}Cu were generated by addition of 2 equiv of the stock to apoproteins and the excess copper was removed by gel filtration chromatography, except for Cu^{II}-H1F-PcoC, which was prepared by direct addition of 0.9 equiv of ^{65}Cu into apoprotein. The samples were concentrated using Millipore Centricon YM-3 centrifugal filter units and the final concentrations were estimated to be approximately 0.8 mM.

EPR spectroscopy

Continuous-wave (CW) experiments were performed using a Bruker ESP380FT/CW X-band spectrometer with a standard rectangular TE_{102} cavity at a microwave frequency of 9.42 GHz. The temperature was maintained at 145 K using a Bruker nitrogen gas flow insert and the microwave frequency was measured with an EIP microwave 548A frequency counter. CW-EPR simulations were performed using the XSophe simulation package [20] running under Mandriva 2007 on an i686 PC. All simulations used exact matrix diagonalization to determine the main transitions in conjunction with high-order perturbation theory to further solve the superhyperfine structure.

Effects of g and A strain were also included in an attempt to properly account for lineshapes.

In some instances the superhyperfine structure could not be fitted unambiguously, with both 3N and 4N coordination being possibilities; the additional outer satellites in the superhyperfine structure and the subtle difference in the intensity profile expected for 4N coordination could not be relied upon to discriminate between 3N and 4N coordination. This is because the overlap of components of the ^{65}Cu $A_{\perp}$ hyperfine structure, together with the choice of A strain parameters $\Delta A_{\|}$ and $\Delta A_{\perp}$, can significantly influence the apparent splittings and intensity profile of the superhyperfine pattern. Additional complications occur if the nitrogen ligands are not assumed to be identical. These additional degrees of freedom may both improve and complicate numerical fitting of the experimental spectrum. The analysis was, therefore, restricted to the assumption of $^{65}Cu^{II}$ coupling to equivalent ^{14}N nuclei. Slightly better fits could be achieved in some instances by adjusting individual ^{14}N parameters by approximately 1–2 MHz from those presented, but because of the aforementioned ambiguity in fitting 3N coordination compared with fitting 4N coordination this was deemed an overinterpretation of the data.

Pulsed-EPR experiments were carried out at approximately 10 K using the ESP380E fitted with a 1-kW TWT amplifier and a Bruker ER 4118 dielectric resonator in an Oxford Instrument CF935 cryostat. Echo-detected EPR spectra were obtained by recording the peak amplitude of the Hahn echo that was generated using the pulse sequence $\pi/2$–Δ–π–Δ-echo as a function of magnetic field. Electron spin echo envelope modulation (ESEEM) spectra were obtained using a three-pulse sequence $\pi/2$–τ–$\pi/2$–t–$\pi/2$-echo, with $t_{\pi/2} = 16$ ns, $\tau = 144$ ns, and a four-step phase cycle to remove unwanted echoes. The time interval t was varied from 32 to 8,224 ns in steps of 32 ns and a four-step phase cycle was used to eliminate unwanted echoes. ESEEM spectra were acquired at discrete magnetic field locations correlating to prominent features in the echo-detected spectra. Hyperfine sublevel correlation experiment (HYSCORE) spectra were obtained using a $\pi/2$–τ–$\pi/2$–t_1–π–t_2–$\pi/2$–τ-echo, with pulse lengths $t_{\pi/2} = 16$ ns and $t_{\pi} = 24$ ns and $\tau = 144$ ns. The time intervals t_1 and t_2 were varied from 48 to 8,240 ns in steps of 64 ns and an eight-step phase cycle was used to eliminate unwanted echoes. Data processing was carried out using the Bruker WinEPR program (version 2.11). The real part of the time-domain spectra was processed by background subtraction of a polynomial function, followed by zero-filling, Hamming apodization, fast Fourier transform and calculation of the absolute value. In the case of the HYSCORE data, the 2D spectrum was also subsequently symmetrized.

Results and discussion

CW-EPR spectroscopy

CW-EPR spectra of the Cu^{II} forms of wild-type, H92F, nA and H1F forms of PcoC are shown in Fig. 2. Superhyperfine structure due to coupling of $^{65}Cu^{II}$ to ligand ^{14}N ($I = 1$) nuclei was apparent in all spectra and clearly resolved in their second-derivative presentations (Figs. 3, 4, 5, 6). This allowed the number of coordinating nitrogen atoms to be estimated from spectral simulations, rather than from Blumberg–Peisach plots [21], which can be ambiguous. The superhyperfine structure in the spectrum of wild-type PcoC could be reproduced satisfactorily assuming coupling to either three or four ^{14}N ligand nuclei (Table 1, Figs. 3, S2, S3). While the 3N model is consistent with the $Cu^{II}(His)_2(N\text{-term})(OH_x)$ ($x = 1$ or 2) site defined previously in the CopC homolog (Fig. 1c) [12], the 4N model raised the possibility of an extra N-amide backbone ligand or substitution of the OH_2 ligand by an unidentified nitrogen ligand from the neighbouring PcoC molecule in the solution. This is possible because both PcoC and CopC are versatile Cu^{I} and Cu^{II} transport proteins with both copper binding sites being highly flexible

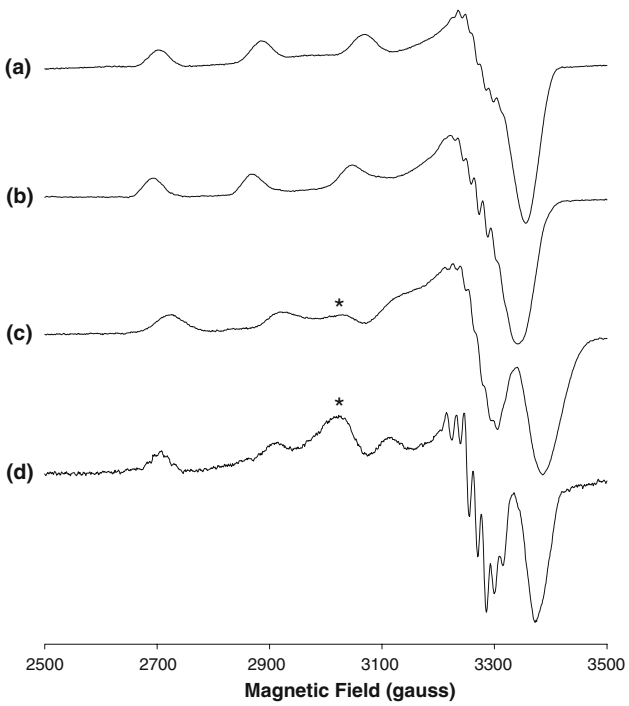

Fig. 2 Frozen-solution continuous-wave electron paramagnetic resonance (EPR) spectra of ^{65}Cu binding to PcoC proteins. *a* wild type, *b* H92F, *c* nA and *d* H1F. An *asterisk* denotes absorption due to additional unidentified species. Experimental conditions were as follows: microwave frequency 9.42 GHz, microwave power 2 mW, modulation amplitude 4 G, sweep time 168 s, time constant 163 ms. *a–c* average of four scans, *d* average of eight scans

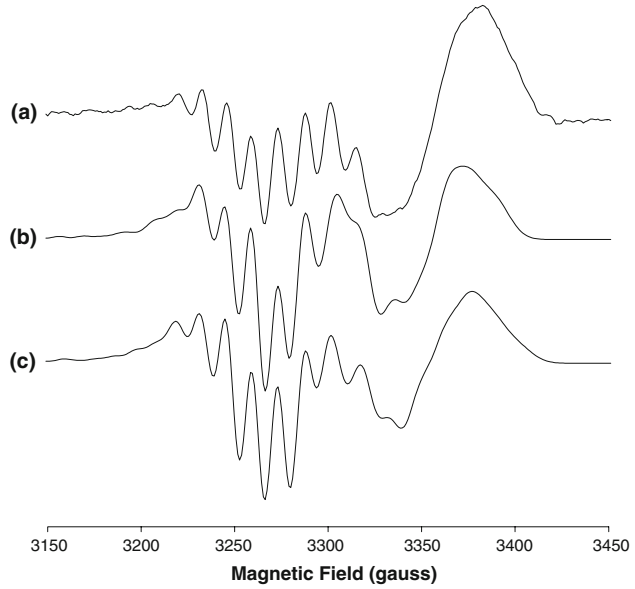

Fig. 3 Comparison of the $g_{\perp}$ region of the second-derivative *a* experimental and *b* and *c* simulated frozen-solution EPR spectra of wild-type PcoC, assuming *b* three and *c* four directly coordinated ^{14}N nuclei. Spin Hamiltonian parameters are given in Table 1. The linewidth parameters were as follows: $\Delta g_{\parallel}/g_{\parallel} = 0.0022$, $\Delta g_{\perp}/g_{\perp} = 0.0017$, $\Delta A_{\parallel} = -2.0 \times 10^{-4}$ cm^{-1}, -2.0×10^{-4} cm^{-1}, residual linewidth 5.0×10^{-4} cm^{-1}

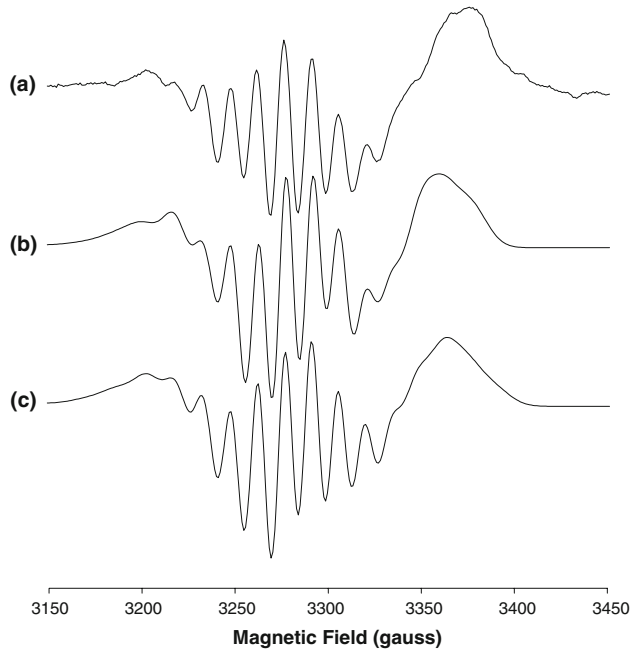

Fig. 4 Comparison of the $g_{\perp}$ region of the second-derivative *a* experimental and *b* and *c* simulated frozen-solution EPR spectra of H92F-PcoC, assuming *b* three and *c* four directly coordinated ^{14}N nuclei. Spin Hamiltonian parameters are given in Table 1. The linewidth parameters were as follows: $\Delta g_{\parallel}/g_{\parallel} = 0.0035$, $\Delta g_{\perp}/g_{\perp} = 0.0023$, $\Delta A_{\parallel} = -5.0 \times 10^{-4}$ cm^{-1}, $\Delta A_{\perp}/A_{\perp} = 2.0 \times 10^{-4}$ cm^{-1}, residual linewidth 5.0×10^{-4} cm^{-1}

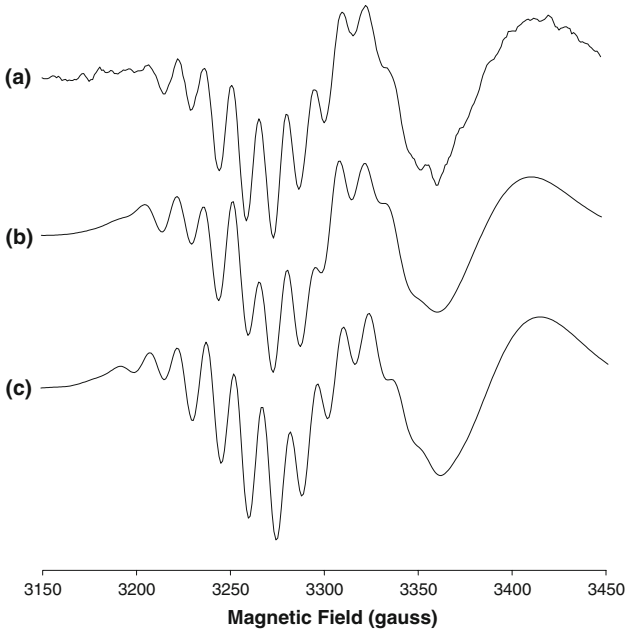

Fig. 5 Comparison of the $g_{\perp}$ region of the second-derivative *a* experimental and *b* and *c* simulated frozen-solution EPR spectra of nA-PcoC, assuming *b* three and *c* four directly coordinated ^{14}N nuclei. Spin Hamiltonian parameters are given in Table 1. The linewidth parameters were as follows: *b* $\Delta g_{\parallel}/g_{\parallel} = 0.0115$, $\Delta g_{\perp}/g_{\perp} = 0.0021$, $\Delta A_{\parallel} = -8.0 \times 10^{-4}$ cm^{-1}, $\Delta A_{\perp}/A_{\perp} = 0.2 \times 10^{-4}$ cm^{-1}, residual linewidth 5.0×10^{-4} cm^{-1}; *c* $\Delta g_{\parallel}/g_{\parallel} = 0.0110$, $\Delta g_{\perp}/g_{\perp} = 0.0021$, $\Delta A_{\parallel} = -7.0 \times 10^{-4}$ cm^{-1}, $\Delta A_{\perp}/A_{\perp} = 0.1 \times 10^{-4}$ cm^{-1}, residual linewidth 5.0×10^{-4} cm^{-1}

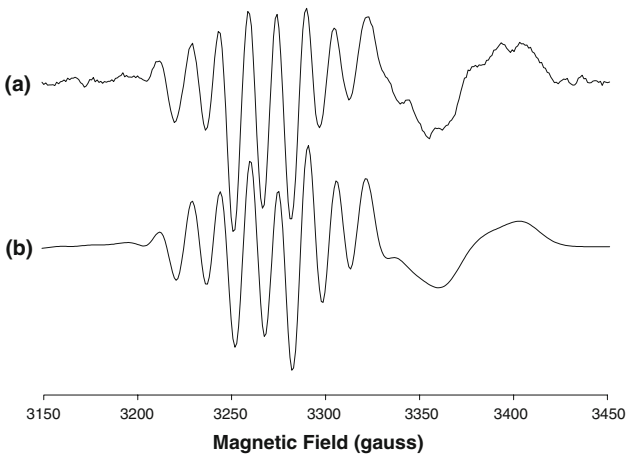

Fig. 6 Comparison of the $g_{\perp}$ region of the second-derivative *a* experimental and *b* simulated frozen-solution EPR spectra of H1F-PcoC, assuming two directly coordinated ^{14}N nuclei. Spin Hamiltonian parameters are given in Table 1. The linewidth parameters were as follows: $\Delta g_{\parallel}/g_{\parallel} = 0.0030$, $\Delta g_{\perp}/g_{\perp} = 0.0015$, $\Delta A_{\parallel} = -5.0 \times 10^{-4}$ cm^{-1}, $\Delta A_{\perp} = 0$, residual linewidth 5.0×10^{-4} cm^{-1}

and solvent-exposed [12, 19]. However, it must be pointed out that while the simulation confirmed a model of at least 3N coordination of the Cu^{II} center, it is difficult to confidently discriminate between 3N and 4N coordination,

Table 1 Spin Hamiltonian parameters of ^{65}Cu binding to PcoC proteins determined from simulation of first- and second-derivative continuous-wave electron paramagnetic resonance spectra

System	$g_{\|\|}$	$g_{\perp}$	$A_{\|\|}$ (^{63}Cu)	$A_{\perp}$ (^{63}Cu)	$A_{\|\|}$ (^{14}N)	$A_{\perp}$ (^{14}N)	^{14}N nuclei
Wild-type PcoC	2.262	2.053	179	8.4	11.0	12.8	3
					10.0	12.8	4
H92F-PcoC	2.276	2.059	176	9.3	11.0	13.5	3
					10.0	13.5	4
nA-PcoC	2.227	2.053	193	15.0	10.0	13.2	3
					10.0	13.4	4
H1F-PcoC	2.233	2.056	199	15.9	12.0	14.5	2

Hyperfine couplings have been converted from ^{65}Cu to those expected for ^{63}Cu and expressed in units of 10^{-4} cm^{-1}. Hyperfine coupling for ^{65}Cu is larger than for ^{63}Cu by a factor of $|g_n(^{65}\text{Cu})/g_n(^{63}\text{Cu})| = 1.07$

because only minor differences between the 3N and 4N models in the numerical simulations were discernable, namely the addition of two extra low-intensity outer satellite lines in the superhyperfine pattern, some unresolved line broadening and a subtle alteration of the intensity ratio of the superhyperfine structure (Figs. 3, S2, S3).

As for the wild-type protein, the key features of the experimental spectrum of H92F-PcoC (Fig. 2, spectrum b) could be obtained by assuming coupling to either three or four equivalent nitrogen ligand nuclei (Table 1, Figs. 4, S4, S5). It is apparent that substitution of ligand His92 with phenylalanine has created an unsaturated Cu^{II} site which forced the metal center to seek alternative ligands, which may involve backbone amide(s) from the highly flexible Cu^{II}-binding loop where His92 is located in the wild-type form. A comparison of the crystal structures of the homologous CopC proteins, $Cu^{I}Cu^{II}$-CopC and apo-H91F CopC variant demonstrated that Cu^{II} binding or mutation of the Cu^{II} site caused little change in the molecular core structure, but significant conformational changes at the Cu^{II} site. The latter is determined mainly by the bidentate His1 ligand in the N-terminus and by His91 in the Cu^{II}-binding loop [12]. However, the similarity of the $g_{\|}$ and $A_{\|}$ parameters of H92F PcoC with those of the wild-type protein suggests that elimination of the His92 ligand perturbs the $^{65}Cu^{II}$ binding site to a lesser extent than that induced by the nA and H1F variations (Table 1, Fig. 2), consistent with the order of their affinities for Cu^{II} [12].

In comparison with the spectra of wild-type and H92F PcoC proteins, the linewidths of nA-PcoC were unusually broad (Fig. 2, spectrum c), as observed previously for this protein [8]. The linewidths of H1F protein were very similar to those of nA-PcoC, but differed distinctly from those of wild-type and H92F forms (Fig. 2). This suggested the presence of a more disordered Cu^{II} site in both the nA and the H1F proteins, apparently attributable to a dramatic perturbation of the strength of the demoted His2 as a crucial bidentate ligand in the former and a complete loss of this bidentate ligand in the latter. Indeed, the dissociation constants of Cu^{II}-H1F PcoC [$K_D(Cu^{II}) > 10^{-5}$ M] and of Cu^{II}-nA-PcoC [10^{-6} M $> K_D(Cu^{II}) > 10^{-13}$ M] are much higher than that of the wild-type form [$K_D(Cu^{II}) \sim 10^{-13}$ M] [19]. The Cu^{II} binding affinities of nA and H1F PcoC have dropped so dramatically that uncharacterized adventitious binding from weaker ligands became competitive, as evidenced from the appearance of a second EPR signal in the nA and H1F spectra (denoted by an asterisk in Fig. 2). For nA-PcoC, it was possible to dramatically reduce this second EPR signal by spectral acquisition immediately after sample generation (Fig. S1). However, this approach was ineffective for the H1F protein, presumably owing to its lower affinity for Cu^{II}. Notwithstanding, divalent copper binding at the Cu^{II} site provided the dominant species for these two proteins and excellent resolution of superhyperfine structure was discernable for the main Cu^{II} species (Fig. 2, spectra c, d), even within the low-field $A_{\|}$ resonance of H1F-PcoC (Fig. 7). In contrast, a single species only was observed for the H92F variant (where a single histidine ligand is eliminated; Fig. 2, spectrum b) and the linewidths and resolution were comparable with those of the wild-type form (Fig. 2, spectra a, b). The available data indicate that the Cu^{II} dissociation constant for this H92F form is intermediate between that of the wild-type protein (high affinity) and the nA variant (low affinity) [19].

The larger linewidths in the nA-PcoC spectrum (Fig. 2, spectrum c) suggested a significant degree of disorder within the Cu^{II} site. Broader $A_{\|}$ features could, in principle, arise from larger unresolved nitrogen hyperfine coupling constants and/or coupling to a larger number of nitrogen ligands. However, the magnitude and multiplicity of the superhyperfine splitting in the perpendicular region is similar to that for wild-type PcoC and so increased strain appears to be the likely cause. Once again, both 3N and 4N simulations produced a plausible reproduction of the experimental spectrum (Table 1, Figs. 5, S6, S7). Previous biophysical characterization of the Cu^{II} form of this protein suggested a $Cu^{II}(His)_2(N/O)_2$ site [8, 18]. It is possible that

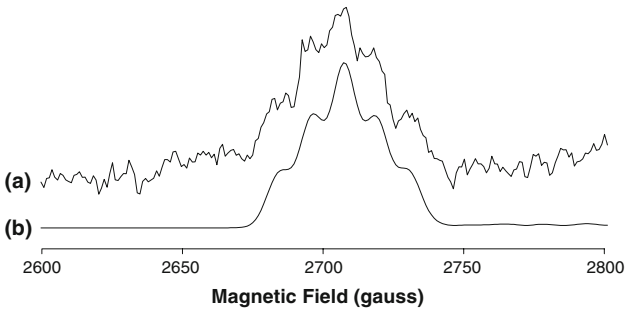

Fig. 7 Superhyperfine structure within the low-field $A_{\|}$ (^{65}Cu) feature of H1F-PcoC. *a* experiment, *b* simulation. Experimental and simulation parameters are the same as those for Fig. 6

the demoted His2 may still bind Cu^{II} but its strength as a bidentate ligand must be perturbed dramatically, if not yet eliminated completely. In addition, the new N-term nitrogen still remains a possibility as an alternative Cu^{II} ligand.

The spectrum of the main Cu^{II} species of H1F-PcoC yielded remarkably well resolved superhyperfine structure, even within the low-field parallel ^{65}Cu hyperfine peak (Figs. 2, spectrum d, 7). For the latter, five lines could be resolved, indicating coupling to just two equivalent nitrogen ligand nuclei. Indeed, a 2N simulation was found to provide an excellent fit of the experimental spectrum (Figs. 6, 7, S8, S9, Table 1). This is in sharp contrast to the 3N/4N model described above for wild-type and H92F PcoC. ESEEM spectroscopy indicates that a single His92 residue still coordinates (vide infra) and thus the other nitrogen-based ligand is likely to be contributed from the N-terminal amine, considering the rigidity of the β-barrel core structure of the molecule and the flexibility of the Cu^{II} site [12]. Remaining non-nitrogen ligands may be contributed by H_2O. Certainly, the dramatic variation in dissociation constants $K_D(Cu^{II})$ (wild type, approximately

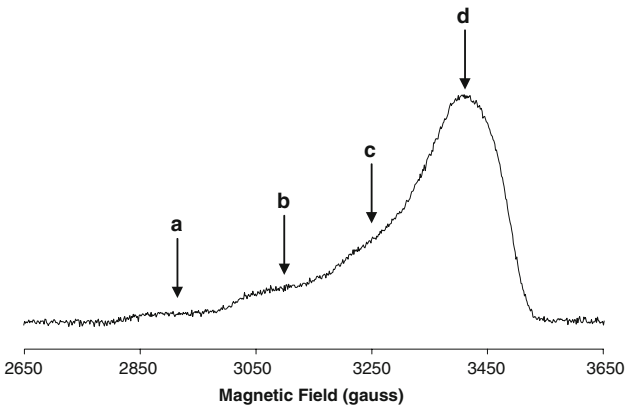

Fig. 8 Echo-detected EPR of ^{65}Cu binding to wild-type PcoC. Three-pulse electron spin echo envelope modulation (ESEEM) experiments were acquired at field positions *a–d*. The experimental parameters were as follows: microwave frequency 9.70 GHz, $t_{\pi/2} = 16$ ns, $t_{\pi} = 32$ ns, $\tau = 200$ ns

10^{-13}; H1F, $>10^{-5}$ M^{-1}) indicates that the Cu^{II} site in H1F-PcoC has been severely disabled.

Pulsed-EPR spectroscopy

To further characterize the Cu^{II} center in wild-type PcoC and to probe the changes of the Cu^{II} site upon protein variations, pulsed-EPR spectroscopy was applied to provide complementary information about the Cu^{II} center. The ESEEM spectra of systems with imidazole ^{14}N coordination from histidine side chains have been well characterized [22, 23]. At X-band frequencies, approximate cancellation of the nuclear Zeeman and nuclear hyperfine interactions takes place, and frequencies characteristic of single-quantum (ν_0, ν_-) and double-quantum (ν_{dq}, ν_+) transitions modulate the decay of the electron spin echo [22, 24]. The ν_0, ν_- and ν_+ frequencies derive from transitions within the α electron spin manifold and ν_{dq} derives from the β manifold. The frequencies are given by

$$\nu_{\pm} = K(3 \pm \eta) \quad (1)$$

$$\nu_0 = 2K\eta \quad (2)$$

$$\nu_{dq} = 2\left[(\nu_I + |A_{iso}|/2)^2 + K^2(3 + \eta^2)\right]^{1/2} \quad (3)$$

where $K = e^2qQ/4h$, A_{iso} is the isotropic ^{14}N hyperfine coupling, ν_I is the ^{14}N Larmor frequency, h is Planck's constant and the asymmetry parameter η lies in the range [0,1]. Deviations from the exact cancellation conditions (Eqs. 1, 2) introduce a small field dependence to each of the abovementioned transitions, while Eq. 3 assumes that the anisotropic hyperfine coupling is small compared with the isotropic interaction, A_{iso}.

Three-pulse ESEEM spectra were acquired at three or four discrete magnetic field locations for the four PcoC proteins (Figs. 8, 9, S10, S11, S12, S13, S14, S15, S16). The resultant frequency-domain spectra of each variant obtained at 3,250 G are shown in Fig. 9, where the three narrow low-frequency single-quantum transitions and the broad double-quantum transition can be identified in the 0–4-MHz range. The broad lineshape between ν_+ and ν_{dq} for all variants can be attributed to the field dependence of the single-quantum transitions within the α submanifold [25, 26].

The "holes" in the ESEEM spectrum of wild-type PcoC at approximately 2.17 and 2.97 MHz can be assigned to combination peaks arising from multiple histidine ligation [26], with the hole near 2.17 MHz being due to $\nu_+ + \nu_0$ and/or $\nu_+ + \nu_-$ and the hole near 2.97 MHz being due to $2\nu_+$ (Fig. 9, spectrum a, Table S1). The appearance of combination frequencies as holes rather than peaks is the result of destructive interference between the narrow combination peak and the broad background, each possessing a different

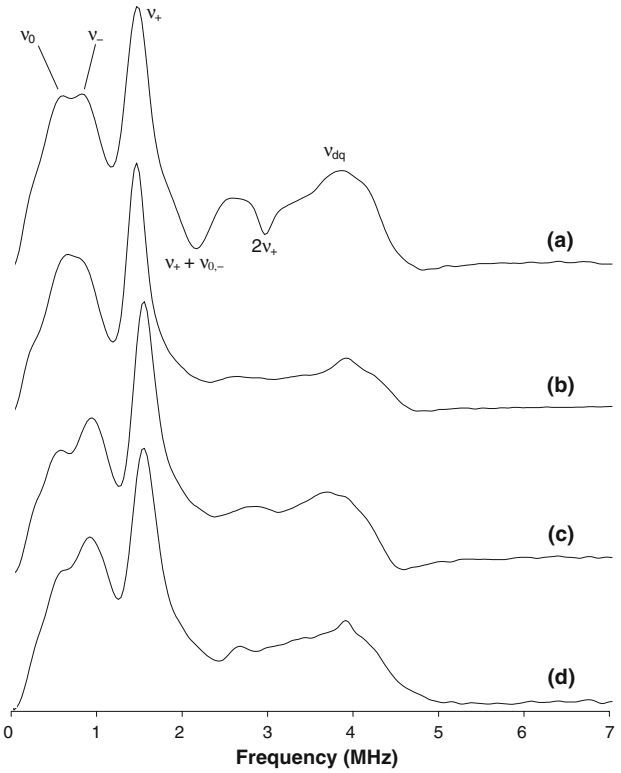

Fig. 9 Three-pulse ESEEM of PcoC proteins at 3,250 G (position c in Fig. 8). *a* wild type, *b* H92F, *c* nA, *d* H1F. The experimental parameters were as follows: microwave frequency 9.70 GHz, $t_{\pi/2} =$ 16 ns, $\tau = 144$ ns, $\Delta t = 32$ ns, $t_0 = 32$ ns. All spectra are normalized by the intensity of the ν_+ transition

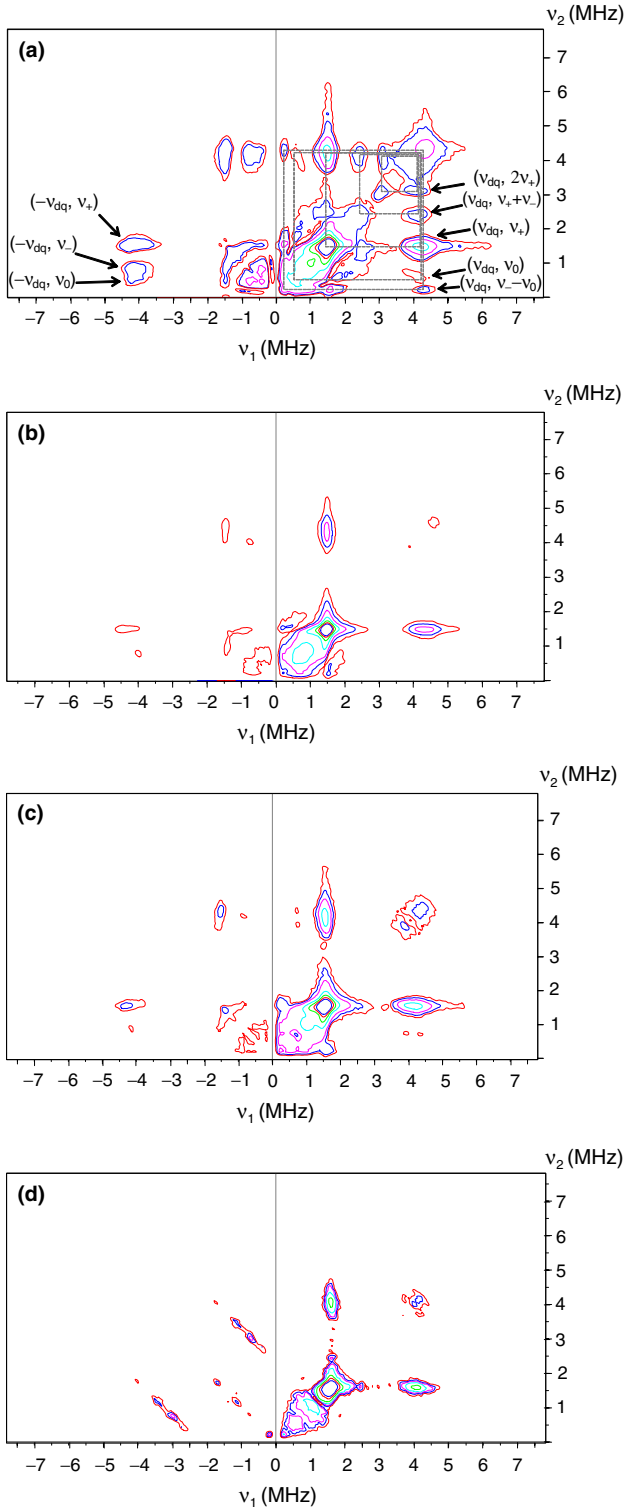

Fig. 10 Hyperfine sublevel correlation experiment spectra of PcoC proteins at 3,400 G near $g_\perp$. **a** Wild type, **b** H92F, **c** nA, **d** H1F. The experimental parameters were as follows: microwave frequency 9.70 GHz, $\tau = 144$ ns, $t_{\pi/2} = 16$ ns, $t_\pi = 24$ ns, $\tau = 144$ ns, $\Delta t_1 = \Delta t_2 = 64$ ns, $t_{10} = t_{20} = 48$ ns

phase. Although the positions of these holes can severely distort absolute-value ESEEM spectra [27]—and they can be effectively eliminated following summation of a large number of spectra with different τ values—we instead obtained subsequent 2D ESEEM (HYSCORE) spectra to more definitively identify the presence of combination peaks.

HYSCORE data were acquired for each PcoC variant near the maximum microwave absorption at 3,400 G (Fig. 8) and the results are shown in Fig. 10. All spectra showed the characteristic cross peaks near (1.5, 4) MHz correlating the double-quantum transitions within each electron spin manifold. Although the cross peak at ($\sim$3.1, $\sim$4) MHz for wild-type PcoC (Fig. 10a) is in the right range for a (ν^{α}_{dq}, ν^{β}_{dq}) transition of a backbone amide nitrogen with $4K =$ 3–4 MHz [28, 29], it also correlates well with ($2\nu_+$, ν_{dq}). Another cross peak at ($\sim$2.3, $\sim$4) MHz further corresponds to ($\nu_+ + \nu_-$, ν_{dq}). This confirms the identity of the "holes" in the three-pulse ESEEM of wild-type PcoC (Fig. 9, spectrum a) as combination peaks. While HYSCORE spectra can be distorted by the same

τ-dependent "holes" that affect three-pulse ESEEM (vide supra), the spatial separation in the second dimension effectively eliminated the destructive interference between the narrow combination peaks and the broad background.

The absence of combination peaks in the H92F and H1F variants (Figs. 9 spectra b, d, 10b, d) is consistent with the presence of a single histidine ligand only for the Cu^{II} center. Since only one histidine has been substituted in each instance, the observation of combination peaks in the wild-type PcoC spectrum confirms that there are two histidine ligands bound to Cu^{II} in the wild-type protein.

The spectrum of the nA protein also appears to lack clear evidence of combination frequencies from multiple histidine coordination (Figs. 9, spectrum c, 10c), consistent with a previous similar observation of Huffman et al. [8] in their three-pulse ESEEM experiment on nA-PcoC. On the basis of their additional electron–nuclear double resonance data, they suggested that two histidine residues may still coordinate Cu^{II} but one may exhibit a very small isotropic hyperfine coupling [8]. In fact, the addition of an extra alanine residue at the N-terminus has changed the nature of the original His1 as a pivotal Cu^{II} ligand so dramatically that both the chemistry and the EPR spectra of nA-PcoC resemble those of H1F-PcoC with an essentially disabled Cu^{II} site, but not those of wild-type and H92F PcoC, which still bind Cu^{II} with high affinity (Fig. 2 in [19]).

The three-pulse ESEEM spectra of wild-type PcoC (Fig. 9, spectrum a) and the H92F variant (Fig. 9, spectrum b) show that the ν_- and ν_0 lines are close together, suggesting that the asymmetry parameter η is large and close to 1. Analysis of the ESEEM frequencies as a function of magnetic field (Figs. S10, S12) under the assumption of exact cancellation conditions (Eqs. 1–3) indicates that the asymmetry parameters are indeed large (Tables S2, S3) and that the quadrupole coupling parameters are consistent with ranges observed previously for imidazole ligands bound to Cu^{II} ($4K \sim 1.5$ MHz and $\eta \sim 0.8$–1) [29]. For wild-type PcoC, comparison of the combination frequencies with the fundamental ν_0, ν_- and ν_+ frequencies (Table S1) suggests that both His1 and His92 have similar nuclear quadrupole parameters. In the case of the H92F variant, the quadrupole parameters may be ascribed to the histidine ligand at position 1. Although the structure of the Cu^{II} binding site in this variant will be perturbed relative to that of the wild-type protein, the similarity of the nuclear quadrupole parameters obtained for H92F-PcoC with those of wild-type PcoC suggests that the coordination of His1 is not greatly affected. In contrast, analysis of the field-dependent three-pulse ESEEM frequencies for nA-PcoC (Figs. S13, S14, Table S4) and H1F-PcoC (Figs. S15, S16, Table S5) reveals an increased K and a decreased η compared with both wild-type PcoC and H92F-PcoC. In particular, the nA variant exhibits a markedly lower η and A_{iso} compared with wild-type PcoC. These observations are consistent with the picture of significant structural perturbations upon eliminating His1 as a Cu^{II} ligand.

Conclusions

The ESEEM experiments confirmed the presence of two histidine ligands at the Cu^{II} site of wild-type PcoC, consistent with the available X-ray crystallographic data for the homolog CopC (Fig. 1c; 67% sequence identity). They also indicated that the surviving histidine residue in the variants H1F and H92F remains as a ligand and that at least one of the two available histidine residues is a ligand in the nA protein.

Fitting of the ^{14}N superhyperfine structure in the CW-EPR spectra confirmed the presence of at least three nitrogen-based ligands at the Cu^{II} sites in three of the four PcoC proteins. The spectra of wild-type PcoC could be fitted adequately with a 3N or a 4N model. The former is consistent with the CopC crystal structure where the N-terminus and side chain of His1 are both bound to the copper ion, making His1 a bidentate ligand, although there is no requirement for the structure obtained in frozen solution to mirror that obtained in the solid state. Hence, our ability to also fit the CW-EPR spectrum of wild-type PcoC to a 4N model indicated that a further backbone amide ligand may be present in the solution form of wild-type PcoC protein studied in the work reported here, rather than the aqua ligand identified in the crystal structure of CopC. Our preliminary EPR studies of CopC (data not shown) are consistent with those reported here for PcoC.

The CW-EPR spectra suggested that the H92F form features at least three nitrogen-based ligands. The spin Hamiltonian parameters of H92F-PcoC are closer to those of wild-type PcoC when compared with the other variants, suggesting a minor perturbation to the Cu^{II} coordination sphere. Hence, the single histidine ligand detected from pulsed-EPR experiments is likely to be the surviving His1 residue. Backbone amide ligands from the highly flexible Cu^{II}-binding loop are presumed to supplement the bidentate His1 in this form.

The CW data confirm the presence of three or four nitrogen-based ligands in the nA form, the latter of which is not inconsistent with a $Cu^{II}(His)_2(N/O)_2$ site suggested from previous X-ray diffraction studies [8, 18]. However, consistent with earlier pulsed-EPR investigation of this variant, only a single histidine ligand could be clearly identified using ESEEM spectroscopy, being the histidine residue at either position 2 or position 93 in the nA form. The significantly different spin Hamiltonian parameters and the larger strain parameters of nA-PcoC compared with

those of the wild-type and H92F forms suggest a less ordered Cu^{II} binding site and reflect the importance of the N-terminal histidine as a bidentate ligand.

The CW-EPR of H1F-PcoC yielded a Cu^{II} site with coupling to two nitrogen-based ligands, with ESEEM spectroscopy showing that one of these ligands was from a histidine side chain, most likely His92. The spin Hamiltonian parameters of H1F-PcoC were most similar to those of the nA form, although the strain parameters of the H1F form were significantly reduced compared with those of both the nA and the wild-type proteins, suggesting a major perturbation of the Cu^{II} binding site in this variant.

In summary, the present results (1) confirm crucial structural differences between the wild type and nA forms (the latter being initially and mistakenly proposed to be the wild-type form [8]), (2) confirm His1 and His92 as ligands in the wild-type form and in addition (3) raise the possibility of a backbone amide nitrogen ligand(s) also being present in the wild-type form, in addition to the N terminus. Taken together, the results provide further evidence in support of the unusual coordination of His1 in the PcoC and CopC proteins.

Acknowledgments We thank Australian Research Council for financial support via grant A29930204. S.C.D. and K.J.B. are funded in part by the National Health and Medical Research Council.

References

1. Rensing C, Grass G (2003) FEMS Microbiol Rev 27:197–213
2. Tetaz TJ, Luke RKJ (1983) J Bacteriol 154:1263–1268
3. Rouch D, Camakaris J, Lee BT, Luke RK (1985) J Gen Microbiol 131:939–943
4. Brown NL, Barrett SR, Camakaris J, Lee BT, Rouch DA (1995) Mol Microbiol 17:1153–1166
5. Cooksey DA (1994) FEMS Microbiol Rev 14:381–386
6. Lee SM, Grass G, Rensing C, Barrett SR, Yates CJD, Stoyanov JV, Brown NL (2002) Biochem Biophys Res Commun 295:616–620
7. Puig S, Thiele DJ (2002) Curr Opin Chem Biol 6:171–180
8. Huffman DL, Huyett J, Outten FW, Doan PE, Finney LA, Hoffman BM, O'Halloran TV (2002) Biochemistry 41:10046–10055
9. Arnesano F, Banci L, Bertini I, Thompsett AR (2002) Structure 10:1337–1347
10. Arnesano F, Banci L, Bertini I, Mangani S, Thompsett AR (2003) Proc Natl Acad Sci USA 100:3814–3819
11. Koay M, Zhang L, Yang B, Maher MJ, Xiao Z, Wedd AG (2005) Inorg Chem 44:5203–5205
12. Zhang L, Koay M, Maher MJ, Xiao Z, Wedd AG (2006) J Am Chem Soc 128:5834–5850
13. Gaggelli E, Kozlowski H, Valensin D, Valensin G (2006) Chem Rev 106:1995–2044
14. Sankararamakrishnan R, Verma S, Kumar S (2005) Proteins 58:211–221
15. Harford C, Sarkar B (1997) Acc Chem Res 30:123–130
16. Djoko KY, Xiao Z, Wedd AG (2008) Chembiochem (in press)
17. Wernimont AK, Huffman DL, Finney LA, Demeler B, O'Halloran TV, Rosenzweig AC (2003) J Biol Inorg Chem 8:185–194
18. Peariso K, Huffman DL, Penner-Hahn JE, O'Halloran TV (2003) J Am Chem Soc 125:342–343
19. Djoko KY, Xiao Z, Huffman DL, Wedd AG (2007) Inorg Chem 46:4560–4568
20. Hanson GR, Gates KE, Noble CJ, Griffin M, Mitchell A, Benson S (2004) J Inorg Biochem 98:903–916
21. Peisach J, Blumberg WE (1974) Arch Biochem Biophys 165:691–698
22. Deligiannakis Y, Louloudi M, Hadjiliadis N (2000) Coord Chem Rev 204:1–112
23. McCracken J, Pember S, Benkovic SJ, Villafranca JJ, Miller RJ, Peisach J (1988) J Am Chem Soc 110:1069–1074
24. Schweiger A, Jeschke G (2001) principles of pulse electron paramagnetic resonance. Oxford University Press, Oxford
25. Mims WB, Peisach J (1978) J Chem Phys 69:4921–4930
26. Jeschke G (1996) Ph.D thesis, Swiss Federal Institute of Technology, Sect 6.3.2
27. Van Doorslaer S, Sierra GA, Schweiger A (1999) J Magn Reson 136:152–158
28. Jin H, Thomann H, Coyle CL, Zumft WG (1989) J Am Chem Soc 111:4262–4269
29. Slutter CE, Gromov I, Epel B, Pecht I, Richards JH, Goldfarb D (2001) J Am Chem Soc 123:5325–5336